RESEARCH ARTICLE | AUGUST 15 2025

Singlet NMR in a case of high molecular symmetry

Urvashi D. Heramun [©] ; Mohamed Sabba; Christian Bengs; Gamal A. I. Moustafa; Malcolm H. Levitt **S**



J. Chem. Phys. 163, 074201 (2025) https://doi.org/10.1063/5.0286843





Articles You May Be Interested In

Nuclear singlet relaxation by chemical exchange

J. Chem. Phys. (September 2021)

Intermolecular vibrations of different isotopologs of the water dimer: Experiments and density functional theory calculations

J. Chem. Phys. (November 2008)

Symmetry effects in rotationally resolved spectra of bi-deuterated ethylene: Theoretical line intensities of *cis*, *trans*, and *as*-C $_2$ H $_2$ D $_2$ isotopomers

J. Chem. Phys. (May 2019)





01 October 2025 13:41:22

Singlet NMR in a case of high molecular symmetry

Cite as: J. Chem. Phys. 163, 074201 (2025); doi: 10.1063/5.0286843

Submitted: 21 June 2025 · Accepted: 24 July 2025 ·

Published Online: 15 August 2025









Urvashi D. Heramun, 🗓 Mohamed Sabba, Christian Bengs, Gamal A. I. Moustafa, and Malcolm H. Levitt 🗓 🗓



AFFILIATIONS

- ¹ School of Chemistry, University of Southampton, Southampton SO17 1BJ, United Kingdom
- ² Department of Chemistry and Materials Science Division, Lawrence Berkeley National Laboratory, University of California Berkeley, Berkeley, California 94720, USA

ABSTRACT

Spin-1/2 pairs support nuclear singlet and triplet states. The mean population difference between the singlet and triplet manifolds is termed singlet order. Under suitable circumstances, nuclear singlet order is highly resistant to several relaxation mechanisms, displaying a decay time constant T_S , which may greatly exceed the time constant T_1 for the equilibration of nuclear magnetization. We explore the nuclear singlet relaxation of an isotopolog of squarate in a high-pH aqueous solution. The $1.3^{-13}C_2$ -isotopolog of squarate exists as a minority species of $1^{-13}C_2$ -squarate. This isotopolog has a high degree of molecular symmetry. ¹⁸O-enrichment is used to generate secondary isotope shifts of the ^{13}C resonances, providing access to $^{13}C_2$ double-quantum coherence and $^{13}C_2$ singlet order. The ^{13}C signals from the $1.2^{-13}C_2$ and $1.3^{-13}C_2$ species are selected using geometric double-quantum filtration, and the double-quantum coherence is converted to singlet order and back again using customized double-quantum-to-singlet (DQ2S) and singlet-to-double-quantum (S2DQ) pulse sequences. We report 13 C₂ singlet lifetime measurements for $1,3-^{13}$ C₂-squarate in a high-pH aqueous solution, in a high magnetic field.

© 2025 Author(s). All article content, except where otherwise noted, is licensed under a Creative Commons Attribution (CC BY) license (https://creativecommons.org/licenses/by/4.0/). https://doi.org/10.1063/5.0286843

I. INTRODUCTION

In high-field nuclear magnetic resonance (NMR), the nuclear spins become slightly polarized when the sample is allowed to reach thermal equilibrium in a strong magnetic field. The time constant for the establishment of thermal nuclear spin polarization is denoted by T_1 . However, this time constant does not always set a fundamental limit on the lifetime of nuclear spin order. In some circumstances, long-lived states (LLS) have been identified, which, in suitable circumstances and in some nuclear spin systems, have much longer lifetimes than T_1 .^{1–33} One prominent example of a LLS is the *singlet* order of pairs of coupled spins-1/2, defined as the population imbalance between the singlet state of the spin pair with total nuclear spin I = 0, and that of the triplet manifold with I = 1, defined as follows:

$$|S_{0}\rangle = (|\alpha\beta\rangle - |\beta\alpha\rangle)/\sqrt{2},$$

$$|T_{+1}\rangle = |\alpha\alpha\rangle,$$

$$|T_{0}\rangle = (|\alpha\beta\rangle + |\beta\alpha\rangle)/\sqrt{2},$$

$$|T_{-1}\rangle = |\beta\beta\rangle.$$
(1)

Here, α and β denote the two spin angular momentum projections $\pm(\hbar/2)$ along an external axis, and the subscripts $M_I \in \{+1, 0, -1\}$ refer to the value of the magnetic spin quantum number.

A prerequisite for the existence of long-lived states is the existence of consistent symmetry in the fluctuating spin Hamiltonian that drives the relaxation process. This means that the fluctuating Hamiltonian is always invariant under one or more permutation operations or geometrical transformations despite its stochastic time-dependence. Consider, for example, an ensemble of isolated spin-1/2 pairs, where the two spins I_i and I_k in each pair only experience their mutual magnetic dipole-dipole coupling. Fluctuations in the orientation and magnitude of the dipole-dipole coupling tensor generate nuclear spin relaxation. The Hamiltonian $\mathcal{H}_{ik}^{D\bar{D}}$ describing the mutual dipole-dipole interaction of the two spins may be written as follows:

$$\mathcal{H}_{ik}^{\mathrm{DD}}(t) = \mathbf{I}_{i} \cdot \mathbf{D}_{ik}(t) \cdot \mathbf{I}_{k}, \tag{2}$$

where the dipole-dipole coupling tensor \mathbf{D}_{ik} is symmetric. Hence, this Hamiltonian is invariant, at all times, to the permutation operation exchanging the two spins:

a) Author to whom correspondence should be addressed: mhl@soton.ac.uk

$$(jk) \mathcal{H}_{jk}^{\mathrm{DD}} (jk)^{\dagger} = \mathcal{H}_{jk}^{\mathrm{DD}}. \tag{3}$$

Here, (jk) denotes the simple swap operator that exchanges the spin I_j with the spin I_k . Even though $\mathcal{H}_{jk}^{\mathrm{DD}}$ fluctuates strongly in time (for a molecule in solution), the symmetry property in Eq. (3) is always preserved. The singlet and triplet states in Eq. (1) span different irreducible representations of the permutation group $\mathcal{G} = \{(), (jk)\}$, where () denotes the identity. Hence, all matrix elements of $\mathcal{H}_{jk}^{\mathrm{DD}}$ between the singlet and triplet states vanish. As a result, the population difference between the singlet and triplet manifolds is immune to relaxation, under these idealized conditions. The same result is obtained by considering the spin quantum numbers I=0 and I=1 for the singlet and triplet states, respectively, and the description of $\mathcal{H}_{jk}^{\mathrm{DD}}$ as a sum of rank-2 irreducible spherical tensor operator components.

In realistic circumstances, perfect permutation invariance is not displayed by all the interactions responsible for spin relaxation, leading to a finite lifetime for long-lived singlet order. In particular, interactions such as the chemical shift anisotropy, and dipolar interactions with additional spins in the same molecule, are not fully permutation-symmetric, except in special cases of particular nuclear locations within molecules of high symmetry.

For example, consider the highly symmetrical squarate dianion $(C_4O_4^{2^-})$, illustrated in Fig. 1. The doubly ^{13}C labeled species $1,2^{-13}C_2$ -squarate, shown in Fig. 1(b), was previously synthesized and studied in solution by ^{13}C singlet NMR. $^{25\ 18}O$ enrichment was used to induce a very small chemical shift difference between the two ^{13}C sites, giving experimental access to the long-lived singlet order.

The singlet decay time constant T_S was previously shown to be strongly pH-dependent due to chemical exchange between the protonated forms.²⁵ In the current work, we concentrate on the high-pH

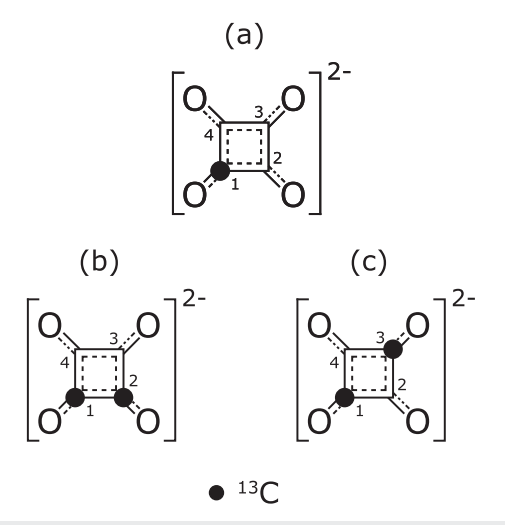


FIG. 1. Molecular structures of the squarate dianion, containing one or two 13 C atoms, indicated by the filled circles. The squarate dianion is the dominant species in high-pH solutions of squaric acid. (a) $^{13}C_1$ -squarate; (b) $1,2^{-13}C_2$ -squarate, as studied in Ref. 25; and (c) $1,3^{-13}C_2$ -squarate. In the current work, double-quantum filtering is used to suppress the 13 C NMR signals of $^{13}C_1$ -squarate, allowing the observation of signals from the $1,2^{-13}C_2$ -squarate and $1,3^{-13}C_2$ -squarate isotopologs.

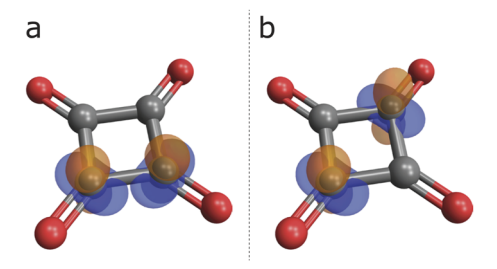


FIG. 2. Ovaloid representations \$^{35,36}\$ of the \$^{13}C\$ CSA tensors, superimposed on the structure of the squarate dianion ($C_2O_4^{2-}$). (a) The ^{13}C CSA tensors of 1,2 $^{-13}C_2$ -squarate. (b) The ^{13}C CSA tensors of 1,3 $^{-13}C_2$ -squarate. Further details on the tensor calculations are given in the supplementary material.

regime, where the squarate dianion is the sole species present in significant concentration.

Since the two 13 C sites in $1,2^{-13}$ C₂-squarate are related by a $\pi/2$ rotation about the molecular C_4 symmetry axis, their CSA tensors have the same eigenvalues (principal values). However, the eigenvectors (principal axes) of the two CSA tensors are not identical, also being related by a $\pi/2$ rotation. This is illustrated in Fig. 2(a), which shows the calculated 13 C CSA tensors of $1,2^{-13}$ C₂-squarate, represented by ovaloids, 35,36 superimposed on the molecular structure. Since the two 13 C tensors have different orientations, the difference between the two CSA tensors, which contributes to the singlet relaxation, 10,12 does not vanish. Hence, although the squarate molecule itself is highly symmetrical, the two 13 C nuclei in $1,2^{-13}$ C₂-squarate are not in sufficiently symmetrical positions to suppress the CSA contribution to singlet relaxation. A similar conclusion applies to the spin-rotation mechanism.

The situation in the $1,3^{-13}C_2$ -squarate isotopolog of Fig. 1(c) is more favorable with respect to the suppression of CSA relaxation. The two 13 C sites of 1,3 $^{-13}$ C₂-squarate are related by a molecular inversion operation. In general, any two molecular sites related by inversion have identical CSA and spin-rotation tensors,³⁷ as shown in Fig. 2(b). Hence, the CSA and spin-rotation contributions to the ${}^{13}C_2$ singlet relaxation of 1,3– ${}^{13}C_2$ -squarate is completely eliminated, within the approximation of rigid molecular geometry. Furthermore, a molecule of 1,3-13C2-squarate contains no other intramolecular relaxation sources since the ¹²C, ¹⁶O and ¹⁸O isotopes all have nuclear spin I = 0. This implies that $1,3^{-13}C_2$ -squarate might be a near-ideal vehicle for the storage of long-lived spin order in solution. The contributions to singlet relaxation are restricted to relatively inefficient intermolecular mechanisms and to residual intramolecular perturbations—caused by temporary geometrical fluctuations, very infrequent protonation events (at high pH), and the possible minor influence of ¹⁸O substitution on the interaction tensors.

A molecular system with approximate local inversion symmetry was previously engineered in the form of a 13 C₂-labeled naphthalene derivative and displayed an exceptionally long singlet relaxation time T_S of more than 1 hour in a degassed non-viscous solvent in low magnetic field. 18 However, that molecular system also contained several spin I=1 deuterium nuclei, which could contribute to residual relaxation processes. The $1,3-^{13}$ C₂-squarate system of Fig. 2(b)

possesses near-ideal inversion symmetry without any other magnetization sources within the same molecule and is also compatible with an aqueous environment—albeit at high pH.

However, a series of technical obstacles lies in the way of accessing and measuring the $^{13}C_2$ singlet order of $1,3-^{13}C_2$ -squarate. The first of these is chemical: although synthetic routes exist for $1^{-13}C_1$ -squarate and $1,2^{-13}C_2$ -squarate, 25 the same is not currently true for the $1,3^{-13}C_2$ isotopolog. Rather than develop the necessary synthetic chemistry, we chose to work with the singly ^{13}C -labeled isotopomer, using the $\sim\!1.1\%$ natural abundance of ^{13}C to provide the second ^{13}C site. This provides simultaneous access to the $1,2^{-13}C_2$ and $1,3^{-13}C_2$ -squarate isotopologs, at the expense of relatively poor signal strength.

The second obstacle is that access to the potentially long-lived $^{13}C_2$ singlet order of $1,3^{-13}C_2$ -squarate requires breaking the chemical equivalence of the two ^{13}C sites, ideally with only a minimum disturbance to the highly symmetrical molecular structure. This condition may be satisfied by substituting one or more ^{16}O atoms by the heavier ^{18}O isotope, which also has nuclear spin I=0. The substitution of one isotope by another of different mass causes small secondary isotope shifts in the chemical shift values. $^{38-44}$ This approach was used previously in the singlet NMR of $^{13}C_2$ -oxalate, $^{15}1,2^{-13}C_2$ -squarate, 25 and the $^{103}Rh_2$ singlet NMR of dirhodium paddlewheel complexes. 32

The third obstacle is that the small 13 C signals from the minor 13 C₂ isotopologs of the singly 13 C-labeled species are readily obscured by the much larger signals from the abundant 13 C₂ species. This obstacle may be overcome by using double-quantum filtration, which is widely used for selective detection of 13 C signals from 13 C₂ species, with suppression of those from 13 C₂ species. 45

In the current case, double-quantum filtering of ¹³C₂ signals encounters a fourth obstacle. The standard techniques for double-quantum excitation in solution NMR require a large chemical shift difference between the coupled spins, relative to the *J*-coupling between them (the "weakly coupled" case).⁴⁵ However, the ¹⁸O-induced secondary ¹³C isotope shifts are small and usually generate ¹³C₂ spin-pair systems in the "near-equivalence" or "extreme strong coupling" limit (the chemical shift frequency difference is much smaller than the *J*-coupling).¹¹ The standard INADEQUATE pulse sequence⁴⁵ has very poor efficiency in the near-equivalence regime. Although the pulse sequence intervals may be extended to deal with strong coupling,⁴⁶ this approach leads to a much longer pulse sequence duration and hence enhanced relaxation losses.

Fortunately, a solution to the problem of double-quantum excitation in the regime of extreme strong coupling is at hand. The technique known as geometric double-quantum excitation (GeoDQ) exploits the geometric Aharanov–Anandan quantum phase to generate double-quantum coherences with high efficiency in near-equivalent spin-1/2 pairs. 47 In the work described in the following, we used GeoDQ to selectively detect the small $^{13}\mathrm{C}_2$ signals of $^{13}\mathrm{C}_2$ -labeled squarate, while suppressing the much larger signals from isolated $^{13}\mathrm{C}$ nuclei. The double-quantum coherences were converted into singlet order by further manipulations, allowing study of the $^{13}\mathrm{C}_2$ long-lived state in the minor isotopologs of $^{18}\mathrm{O}$ -enriched $^{13}\mathrm{C}_2$ -squarate.

In the rest of this paper, we describe a series of ¹³C NMR observations on an aqueous solution of ¹⁸O-enriched 1-¹³C-squarate. A rich spectral pattern is observed due to the pH-dependent

 $^{18}\mathrm{O}$ -induced secondary isotope shifts of the $^{13}\mathrm{C}$ resonances and the many possible $^{18}\mathrm{O}$ isotopologs. As described in the following, the evidence indicates that the pH-dependence of the $^{18}\mathrm{O}$ -induced $^{13}\mathrm{C}$ isotope shifts is not only due to the $^{18}\mathrm{O}$ -induced perturbations of the vibrational wavefunctions but also due to perturbations of the acid-base equilibria by the substitution of $^{18}\mathrm{O}$ for $^{16}\mathrm{O}$. We demonstrate the successful implementation of geometric double-quantum excitation to selectively detect the $^{13}\mathrm{C}$ NMR signals from $^{18}\mathrm{O}$ isotopologs of $1,2^{-13}\mathrm{C}_2$ and $1,3^{-13}\mathrm{C}_2$ -squarate. This made it possible to determine the $^{13}\mathrm{C}_2$ singlet lifetimes of both $^{13}\mathrm{C}_2$ isotopologs of the squarate di-anion, in a high magnetic field.

II. MATERIALS AND METHODS

A. Sample preparation

The samples consisted of 4.6 mg of 1^{-13} C-squaric acid, dissolved in 400 μ l of a 1:1 mixture of H_2^{-18} O: D_2^{-16} O to make up a 0.1M solution. The isotopic purity of H_2^{-18} O was 97.1%. The solutions were incubated at 80 °C for two hours to allow the 16 O/ 18 O exchange process to reach a dynamic equilibrium. Samples with differing pH values were prepared by step-wise addition of a 2M solution of sodium hydroxide. For each instance, the volume did not exceed 65 μ l, and therefore, any effects on sample concentration were deemed negligible. The pH measurements were carried out with a Hamilton SpinTrode pH electrode (www.hamiltoncompany.com). The calibration of the pH meter was verified over the full pH range, using standard buffers. When degassing is indicated, this was achieved by a standard freeze-pump-thaw procedure under an inert atmosphere for ten total cycles.

B. NMR instrumentation

The solution-state NMR experiments were carried out on a Bruker Neo Avance 400 MHz system equipped with a 5 mm Bruker BBO probe and a Bruker Neo Avance 700 MHz system equipped with a Bruker TCI prodigy 5 mm cryoprobe. The 90° pulse length τ_{90} was optimized to 9.15 ± 0.1 μ s at 400 MHz and 12.75 ± 0.1 μ s at 700 MHz.

III. RESULTS

A. ¹³C NMR spectra

The 13 C spectrum of the 18 O-enriched 1^{-13} C-squarate solution takes the form of 12 closely-spaced peaks, as shown in Fig. 3(b). The mean chemical shift of the multiplet shifts downfield (i.e., high values of chemical shift δ) as the pH is increased, as shown in Fig. 3(a). The mean 13 C chemical shift changes by ~+7.7ppm when the pH is increased from 0.9 to 13.3.

The pH-dependence of the ^{13}C chemical shift is due to the dynamic equilibrium of the squarate dianion with the conjugate acids mono-hydrogen squarate $(C_2O_4H^-)$ and the di-protonated neutral species squaric acid $(C_2O_4H_2)$, as shown in Fig. 4. The observed ^{13}C chemical shift is a population-weighted average of the ^{13}C shifts of the rapidly exchanging species in solution. This leads to a strong pH-dependence of the mean ^{13}C chemical shift, as shown in Fig. 3(a).

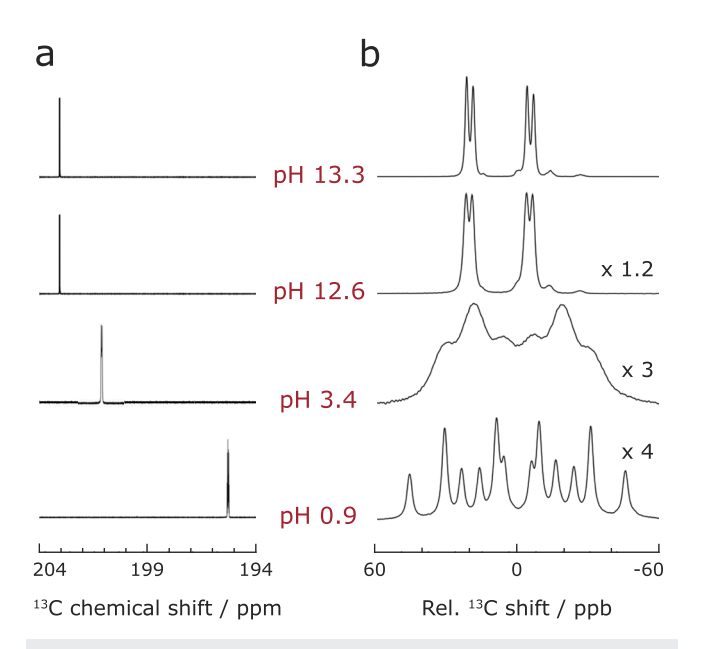


FIG. 3. (a) Variation in the 13 C chemical shift positions as a function of pH for samples of 18 O-enriched 13 C₁-squaric acid dissolved in 1:1 H₂ 18 O:D₂ 16 O. Each spectrum was acquired for 200 transients at 9.4 T and 298 K. (b) Expansion of the relevant spectral region for each pH point shown, spanning 120 ppb. The chemical shift scale at pH 0.9 is centered around 195.32 ppm, 201.12 ppm at pH 3.4, and 203.05 ppm at pH 12.6 and pH 13.3. The vertical scales are given with respect to the pH 13.3 spectrum.

Figure 3(b) shows expanded views of the 12-peak multiplet as a function of pH. Note that the frequency axes of the four spectra in Fig. 3(b) are centered at different chemical shift values, as described in the caption. The 12 multiplet components are quite well-resolved at pH = 0.9, with the multiplet pattern spanning almost 50ppb. The spectrum at pH = 3.4 is strongly broadened. At high pH values the 13 C spectrum takes the form of two well-separated doublets, flanked by small additional features which are attributed to minor isotopologs with two 13 C nuclei, as discussed in detail in the following.

As is clear from Fig. 3(b), the ¹⁸O-induced secondary ¹³C isotope shifts are strongly pH-dependent. There are two relevant mechanisms for the secondary isotope shifts.

- 1. Vibronic mechanism. Observed chemical shifts are averages over vibrational wavefunctions; since vibrational wavefunctions are modified by changing the mass of the participating atoms, isotopic substitution slightly modifies the vibrationally averaged chemical shifts. This mechanism has been documented thoroughly. 38-42 The theory is well-developed, even including relativistic effects. 43,44 Vibronic secondary isotope shifts often become smaller in magnitude as the number of bonds separating the participating atoms increases. However, this is not always the case, as is shown in the following.
- 2. *Dynamic mechanism*. For chemically exchanging systems, in the fast exchange regime, the observed chemical shifts are population-weighted averages over the chemical shifts of

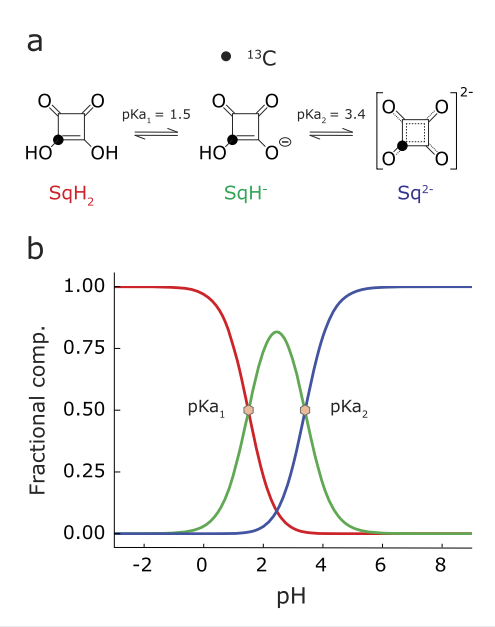


FIG. 4. (a) Dynamic equilibrium displayed by 13 C₁-squaric acid in a solution. The diprotic squaric acid SqH₂ (red) is most abundant below pKa₁ = 1.5, while the squarate dianion Sq²⁻ (blue) dominates beyond pKa₂ = 3.4. Between the two extremes is the singly protonated species hydrogen squarate SqH⁻ (green). (b) Fractional composition diagram showing the distribution of the various species of squaric acid at different pH values. Each pKa value equals the pH at the corresponding half-equivalence point.

the relevant chemical species. Replacement of ¹⁶O by ¹⁸O modifies the equilibrium concentrations of the exchanging species, for example, by changing the zero-point energy of O-H bond vibrations, effectively modifying the acidity of the affected -OH group. 48,49 Since the observed chemical shift depends on the equilibrium concentrations of the exchanging species, isotopic substitution can lead to chemical shift changes, even remote from the site of isotopic substitution. Here, this effect is called the dynamic isotope shift mechanism. In suitable cases, dynamic isotope shifts may be much larger than vibronic isotope shifts, may be observed much further from the site of isotopic substitution than vibronic isotope shifts, and may have the opposite sign to vibronic shifts. So far, the dynamic isotope shift mechanism has not been as thoroughly examined as the vibronic mechanism, although its importance has been identified in some cases. 42,48-51 Some reports of unusually large and unexplained isotope shifts may probably be attributed to the dynamic mechanism.⁵²

In the current system, the ¹⁸O-induced secondary ¹³C isotope shifts are caused by a superposition of the vibronic and dynamic mechanisms. A detailed analysis is deferred to a future report.

In the following discussion, the secondary isotope shifts are described by the following convention, as used in recent papers: 15,25

$$^{n}\Delta X(h) = \delta_{X}(h) - \delta_{X}(l). \tag{4}$$

Here, Δ represents the chemical shift difference induced by substitution; X is the nucleus being observed; h is the heavier isotope; l is the

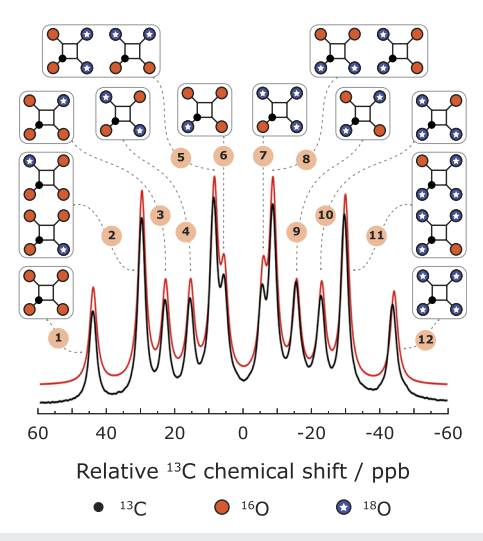


FIG. 5. Isotopologs of ¹⁸O-enriched ¹³C $_1$ -squarate and their correspondence with the ¹³C spectrum at pH 0.9. The filled black circles denote ¹³C atoms. The filled orange circles denote ¹⁶O atoms, while the blue stars denote ¹⁸O atoms. The experimental spectrum at 9.4 T (black, 512 scans), is compared to a simulation of the spectrum (red). The ¹³C chemical shift scale is centered at 195.32 ppm.

lighter isotope; and n is the number of chemical bonds separating X and h. This convention is intuitive since it indicates the change in chemical shift when the most common isotope is replaced by a heavier one, although some literature uses the opposite sign.⁴¹

1. 13 C spectrum at pH 0.9

A detailed view of the 13 C spectrum of the 18 O-enriched 1^{-13} C-squarate solution at pH = 0.9 is shown in Fig. 5, together with the assignments of the 12 peaks to the 18 O isotopologs. Because of the molecular symmetry, some isotopologs, such as 1^{-13} C, 2^{-18} O-squarate (peak 2), are twice as probable as some others, such as 1^{-13} C, 3^{-18} O-squarate (peak 3). Peak 2, therefore, has twice the intensity of peak 3. The probability of a given isotopolog is called here the *statistical weight*. The isotopolog 1^{-13} C, 2^{-18} O-squarate has twice the statistical weight of the isotopolog 3^{-18} O-squarate.

Table I displays the set of ¹⁸O-induced ¹³C secondary isotope shifts, which is consistent with the observed spectrum at pH 0.9. A simulation of the spectrum, using the isotope shifts in Table I and the statistical weights of the isotopologs, is also shown in Fig. 5. This simulation assumes that the secondary isotope shifts are additive. The secondary isotope shift of a ¹³C nucleus, which is one bond away

TABLE I. Experimentally measured secondary isotope shifts for 18 O-enriched 13 C₁-squarate at pH 0.9 (Fig. 5), in a magnetic field of 9.4 T and a sample temperature of 298 K. The isotope shift convention is given in Eq. (4).

¹³ C isotope shift	Value (ppb)	
$^{1}\Delta^{13}C(^{18}O)$ $^{2}\Delta^{13}C(^{18}O)$ $^{3}\Delta^{13}C(^{18}O)$	-40.1 ± 0.5 -14.9 ± 0.5 -22.1 ± 0.5	

from one ¹⁸O atom and two bonds away from a second ¹⁸O atom, experiences a secondary isotope shift of ¹ Δ ¹³C (¹⁸O) +² Δ ¹³C (¹⁸O), and similarly for all the other isotopologs. The agreement with the experimental spectrum is good.

Note that the secondary isotope shifts in Table I do not show a monotonic dependence on the number of bonds n separating the atoms, with the two-bond shifts being smaller in magnitude than the three-bond shifts. All isotope shifts are negative, meaning that the substitution of $^{16}\mathrm{O}$ by the heavier $^{18}\mathrm{O}$ isotope leads to a decrease in the $^{13}\mathrm{C}$ chemical shift δ , i.e., a "high-field" shift. The peak of the $^{16}\mathrm{O_4}$ isotopolog, therefore, has the highest δ value and appears on the extreme left of the $^{13}\mathrm{C}$ multiplet, while the peak of the $^{18}\mathrm{O_4}$ isotopolog appears on the extreme right. We are confident that no other combinations of isotope shifts match the observed spectra.

2. 13 C spectrum at pH 3.4

The ^{13}C spectrum at pH $\simeq 3.4$ is shown in Fig. 3(b). The spectral peaks are relatively broad, presumably because the protonation and deprotonation events occur, at this pH value, on a similar time scale to the inverse of the exchange-induced changes in the ^{13}C resonance frequency. This spectrum was not analyzed further.

3. ¹³C spectrum at pH 13.3

At high pH values, the ¹³C spectrum of the ¹⁸O-enriched 1-¹³C-squarate solution displays four strong peaks, arranged as two well-separated doublets. The assignments of the four ¹³C peaks to the ¹⁸O isotopologs of 1-¹³C-squarate are shown in Fig. 6. The ¹⁸O-induced secondary isotope shifts at high pH are given in Table II. At this pH value, only the deprotonated squarate

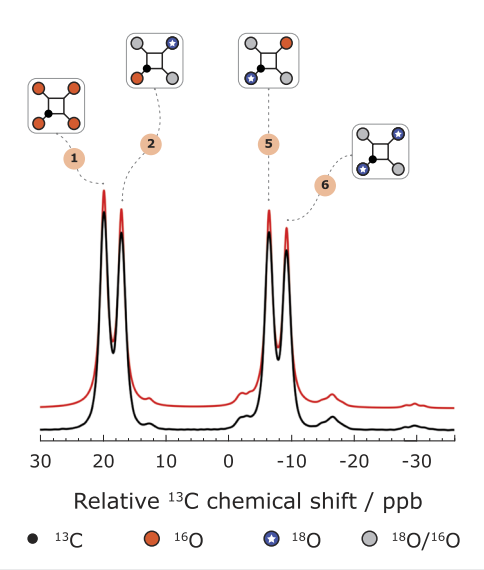


FIG. 6. ¹⁸O isotopologs of ¹³C₁-squarate, and their correspondence with the ¹³C spectrum at pH 13.3. The filled black circles denote ¹³C atoms. The filled orange circles denote ¹⁶O atoms, while the blue stars denote ¹⁸O atoms. The filled gray circles denote oxygen atoms, which may be either ¹⁶O or ¹⁸O; since the two-bond isotope shift ² Δ ¹³C (¹⁸O) is negligible (see Table II), the isotopic nature of these oxygen atoms does not affect the ¹³C spectrum. The experimental spectrum at 9.4 T (black, 512 scans) is compared to a simulation of the spectrum (red). The ¹³C chemical shift scale is centered at 203.05 ppm.

TABLE II. Estimated values of the ^{18}O and ^{13}C -induced ^{13}C isotope shifts of ^{18}O -enriched $^{13}C_1$ -squarate at pH 13.3 (Figs. 6 and 7) at 9.4 T and 298 K. Note the negligible magnitude of the two-bond ^{18}O -induced isotope shift $^2\Delta^{13}C(^{18}O)$. The isotope shift convention is given in Eq. (4).

¹³ C isotope shift	Value (ppb)	
$^{1}\Delta^{13}C(^{18}O)$ $^{2}\Delta^{13}C(^{18}O)$ $^{3}\Delta^{13}C(^{18}O)$	-25.7 ± 0.5 0.0 ± 0.5 -2.7 ± 0.5	
$^{1}\Delta^{13}C(^{13}C)$ $^{2}\Delta^{13}C(^{13}C)$	-21.3 ± 0.5 -7.1 ± 0.5	

dianion is present in appreciable concentration. Hence, the high-pH $^{13}\mathrm{C}$ isotope shifts may be attributed solely to the vibronic mechanism.

Surprisingly, the two-bond secondary isotope shift $^2\Delta^{13}C(^{18}O)$ is found to be indistinguishable from zero, at high pH. There is no other feasible interpretation for the two-doublet form of the high-pH ^{13}C spectrum. At present, the surprisingly low value of the two-bond ^{18}O -induced vibronic ^{13}C isotope shift is unexplained. This observation is possibly associated with the high symmetry of the molecule.

The high-pH spectrum also displays smaller features which are attributed to low-abundance isotopologs containing pairs of 13 C nuclei. The assignments of these peaks to sets of isotopologs are shown in Fig. 7, together with a simulation of the spectrum using the isotope shift values in Table II. The 13 C peaks of the 13 C₂-isotopologs

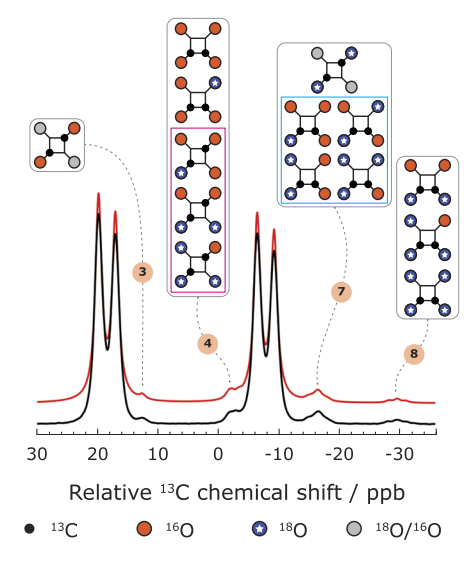


FIG. 7. ¹⁸O isotopologs of ¹³C₂-squarate and their correspondence with the ¹³C spectrum at pH 13.3. The filled black circles denote ¹³C atoms. The filled orange circles denote ¹⁶O atoms, while the blue stars denote ¹⁸O atoms. The filled gray circles denote oxygen atoms, which may be either ¹⁶O or ¹⁸O. The experimental spectrum at 9.4 T (black, 512 scans) is compared to a simulation of the spectrum (red). The ¹³C chemical shift scale is centered at 203.05 ppm.

are shifted to low δ values ("high-field"), relative to those of the $^{13}C_2$ species, by the secondary ^{13}C isotope shift induced by the presence of a ^{13}C neighbor. The experimentally determined $^{1}\Delta^{13}C(^{13}C)$ and $^{2}\Delta^{13}C(^{13}C)$ isotope shifts are given as the last two rows of Table II. The spectral simulations assume that all secondary isotope shifts are additive.

Simulations of the spectra, using the isotope shifts in Table II and the known statistical weights of the isotopologs, are also shown in Figs. 6 and 7. These simulations assume that the secondary isotope shifts are additive. In cases where there are spectral contributions from chemically inequivalent $^{13}C_2$ pairs, the simulations included all four peaks of the corresponding AB spin system, using the predicted ^{18}O -induced isotope shifts for the two ^{13}C nuclei and estimated values of J_{CC} from computational chemistry (see Table III). The agreement with the experimental spectra is good.

There are two sets of isotopologs that are particularly interesting from the point of view of the current paper. These are the ¹³C₂ isotopologs for which one ¹³C atom has ¹⁸O as a directly bonded neighbor, while the other ¹³C atom has ¹⁶O as a directly bonded neighbor. In these cases, the asymmetrical ${}^{1}\Delta^{13}C({}^{18}O)$ secondary isotope shifts break the chemical equivalence of the two ¹³C nuclei, providing access to ¹³C₂ singlet order and ¹³C₂ double-quantum coherence. $1,2^{-13}C_2$ -squarate isotopologs of this type contribute to the peak cluster at position 7 in Fig. 7, while the relevant 1.3^{-13} C₂squarate isotopologs contribute to peak 4. Note, however, that in both cases, the relevant signals almost coincide with those from isotopologs of less interest. In the case of peak 7, the signals of interest from the 1,2-13C2, 1-18O, 2-16O species almost coincide with the from the 1,2⁻¹³C₂, 1⁻¹⁶O, 2⁻¹⁶O species almost coincide with the signals from 1,3⁻¹³C₂, 1,3⁻¹⁸O₂ species; In the case of peak 4, the signals from 1,3⁻¹³C₂, 1⁻¹⁸O, 3⁻¹⁶O species almost coincide with those from 1,2⁻¹³C₂, 1,2⁻¹⁸O₂ species. Furthermore, in the case of 1,3⁻¹³C₂-squarate, the relevant 13 C peaks are close in frequency to the peak from isotopologs of 1^{-13} C, 1^{-18} O, 3^{-16} O-squarate, which is present in much higher abundance (peak 5 in Fig. 6). In order to observe the ¹³C spectra of the most interesting isotopologs cleanly, it is, therefore, necessary to suppress the overlapping signals from the less desirable ones.

TABLE III. First three rows: pulse sequence parameters used for the geometric double-quantum filtration experiments at 16.4 T and 298 K for a pH 13.3 sample. Next four rows: spin system parameters deduced from the optimized values of the pulse sequence parameters, using Eqs. (6)–(8). The small values of $\theta_{\rm ST}$ indicate $^{13}{\rm C}_2$ spin pairs in the near-equivalence regime. Last row: estimated values of the $^{13}{\rm C}^{-13}{\rm C}$ *J*-couplings by a range of computational chemistry methods (see the supplementary material).

Parameter	$1,2^{-13}C_2$ -sq.	$1,3-^{13}C_2$ -sq.
τ_1/ms	4.53	6.21
τ_2/ms	9.06	12.42
n	20	16
J/Hz	55.0 ± 0.1	40.1 ± 0.1
$\Delta\delta$ /ppb	5.8 ± 0.1	5.8 ± 0.1
$\Omega/(2\pi)/Hz$	55.2 ± 0.1	40.3 ± 0.1
$\theta_{\rm ST}/^{\circ}$	4.2 ± 0.2	5.8 ± 0.2
J _{calc} /Hz	56.5 ± 0.5	47.8 ± 0.5

n times

B. Double-quantum filtered NMR

There are several methods for selecting the NMR signals from spin-1/2 pairs, while suppressing the signals from isolated spins-1/2. The standard method is double-quantum-filtration, which has long been used for the selective detection of $^{13}\mathrm{C}_2$ signals. 45,54 An alternative method is singlet-order filtration, which exploits the isotropic rotational properties of singlet order, rather than using double-quantum coherence, 23,55 and which has been performed in vivo. 27,31 As described in the supplementary material, we explored both techniques, but found the double-quantum-filtration method to be superior in the current case, for which the large $^{13}\mathrm{C}$ signals from the $^{13}\mathrm{C}_2$ isotopologs present a significant challenge.

In the cases of interest, the resonance frequency difference between the ^{13}C nuclei of the $1,2^{-13}\text{C}_2$ and $1,3^{-13}\text{C}_2$ squarate isotopologs is small. This leads to $^{13}\text{C}_2$ pair systems of the nearequivalent AB type. For example, in a field of 16.4 T, the $^1\Delta^{13}\text{C}(^{18}\text{O})$ secondary isotope shift of $\sim\!-25.7$ ppb leads to a resonance frequency change of 4.52 Hz, which is much smaller than the estimated ^{13}C - ^{13}C J-couplings of 55.0 Hz for the $1,2^{-13}\text{C}_2$ isotopologs and 40.1 Hz for the $1,3^{-13}\text{C}_2$ isotopologs (see Table III).

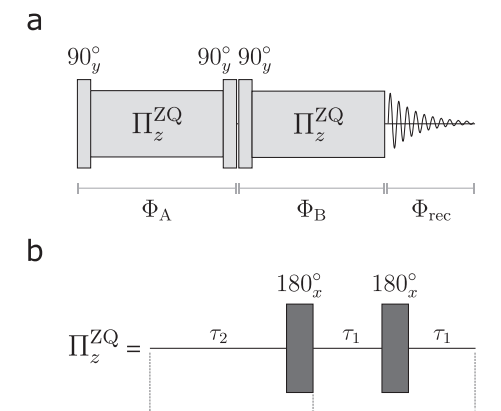
The relevant ¹³C₂ spin pairs, therefore, form very strongly coupled AB systems. The standard INADEQUATE pulse sequence for double-quantum excitation⁴⁵ is not suitable for this coupling regime. The INADEQUATE pulse sequence may be adapted for the strong coupling case by greatly extending the pulse sequence duration.⁴⁶ However, this approach leads to considerable relaxation losses.

We, therefore, employed the geometric double-quantum (GeoDQ) excitation procedure, which was recently shown to be effective for double-quantum excitation in near-equivalent AB spin systems.⁴⁷ The double-quantum excitation procedure is shown in Fig. 8 and employs two $\pi/2$ pulses bracketing a sequence denoted $\Pi_z^{\rm ZQ}$, which leads to an effective π rotation about the z axis of the zero-quantum subspace spanned by the singlet state $|S_0\rangle$ and the central triplet state $|T_0\rangle$ of the strongly coupled AB system [Eq. (1)]. The propagator for this sequence, in the basis of singlet and triplet states [Eq. (1)], is given by

$$\Pi_z^{\text{ZQ}} = \begin{pmatrix} -i & 0 & 0 & 0 \\ 0 & 1 & 0 & 0 \\ 0 & 0 & +i & 0 \\ 0 & 0 & 0 & 1 \end{pmatrix}.$$
(5)

The Π_z^{ZQ} sequence inscribes a cyclic "spherical lune" trajectory on the Bloch sphere of the zero-quantum transition, with an opening angle of $\pi/2$, so that the trajectory subtends a solid angle of π at the origin.⁴⁷ This geometrical property invests the connected single-quantum coherences with opposite phase shifts of $\pm \pi/2$, permitting the excitation of double-quantum coherence by a subsequent $\pi/2$ pulse.⁴⁷ The phase shift of the $|T_0\rangle$ state induced by the Π_z^{ZQ} sequence, which is associated with the solid angle subtended by the zero-quantum Bloch-sphere trajectory, is a manifestation of the geometric Aharanov–Anandan phase, 47,56 a non-adiabatic generalization of Berry's phase. 57,58

The timings of the GeoDQ sequence depend on the parameters Ω and $\theta_{\rm ST}$, which are defined as follows in terms of the parameters of the near-equivalent spin-1/2 pair:



n times

FIG. 8. (a) Geometric double-quantum-filtering pulse sequence. The pulse sequence consists of two blocks, with overall phases Φ_A and Φ_B , which are cycled together with the receiver phase $\Phi_{\rm rec}$ in order to select signals passing through (± 2)-quantum coherence between blocks A and B. The double-quantum excitation block A consists of two $\pi/2$ pulses bracketing a sequence labeled $\Pi_z^{\rm ZQ}$, which generates a rotation through the angle π about the z axis of the zero-quantum space [Eq. (5)]. The double-quantum reconversion block B consists of a single $\pi/2$ pulse, followed by an identical $\Pi_z^{\rm ZQ}$ sequence. The phases of the blocks are cycled as an overall four-step cycle: $\Phi_A = \{0,0,0,0\}, \Phi_B = \{0,\pi/2,\pi,3\pi/2\},$ and $\Phi_{\rm rec} = \{0,3\pi/2,\pi,\pi/2\}$. (b) Each $\Pi_z^{\rm ZQ}$ sequence consists of two elements, each of which is repeated n times, before proceeding to the next element. The first element consists of an interval τ_2 , followed by a π pulse, with the delay-pulse sequence repeated n times. The second element consists of a delay τ_1 , a π pulse, and another delay τ_1 , with the delay-pulse-delay sequence repeated n times. The darker color indicates a composite 180° pulse. The horizontal expressions for τ_1 , τ_2 , and n are given in Eq. (8). The parameters used in the experiments are given in Table III.

$$\Omega = \sqrt{\omega_I^2 + \omega_\Delta^2},$$

$$\theta_{ST} = \arctan\left(\frac{\omega_\Delta}{\omega_I}\right).$$
(6)

The chemical shift frequency difference ω_{Δ} and *J*-coupling are given in angular units by

$$\omega_{\Delta} = \Delta \delta \times \omega^{0},$$

$$\omega_{I} = 2\pi I,$$
(7)

where $\Delta\delta$ is the difference in chemical shifts and $\omega^0 = -\gamma B^0$ is the nuclear Larmor frequency of the homonuclear spin pair. The angle $\theta_{\rm ST}$ is the singlet–triplet mixing angle and is small in magnitude for a near-equivalent AB system, approaching $\pi/2$ for the weak-coupling AX case. The current spin systems all have small values of $\theta_{\rm ST}$, as shown in Table III.

Theoretical expressions for the pulse sequence intervals τ_1 and τ_2 , and the loop number n, are given by⁴⁷

$$\tau_1 = \pi/(2\Omega),$$

$$\tau_2 = 2\tau_1,$$

$$n = 2 \times \text{round}(\pi/(4\theta_{ST})).$$
(8)

The last equation ensures that n is an even number, which leads to the most robust performance.⁵⁹ In practice, these parameters were optimized experimentally. The experimental parameters are given in Table III.

A double-quantum-filtered ^{13}C NMR spectrum of the ^{18}O -enriched $1^{-13}C$ squarate solution at high pH is shown in Fig. 9(b). This spectrum was obtained using the geometric double-quantum-filtering pulse sequence of Fig. 8, using the parameters of Table III (center column), which are optimized for the detection of the $1,2^{-13}C_2$ -squarate isotopolog. As may be seen in Fig. 9(b), the selective detection of the small $1,2^{-13}C_2$ -squarate signal, and the suppression of the large $^{13}C_2$ signals, is excellent.

Figure 10(b) shows a similar spectrum, obtained by using the parameters of Table III (right column), which are optimized for the detection of the $1,3^{-13}C_2$ -squarate isotopolog. In this case, the $1,3^{-13}C_2$ -squarate signal is observed with high efficiency. The $1,2^{-13}C_2$ -squarate signal also appears in this spectrum, albeit with reduced intensity. This is expected, since the double-quantum filter allows signals of both $^{13}C_2$ pairs to pass. The suppression of the $^{13}C_2$ signals is excellent in this case too.

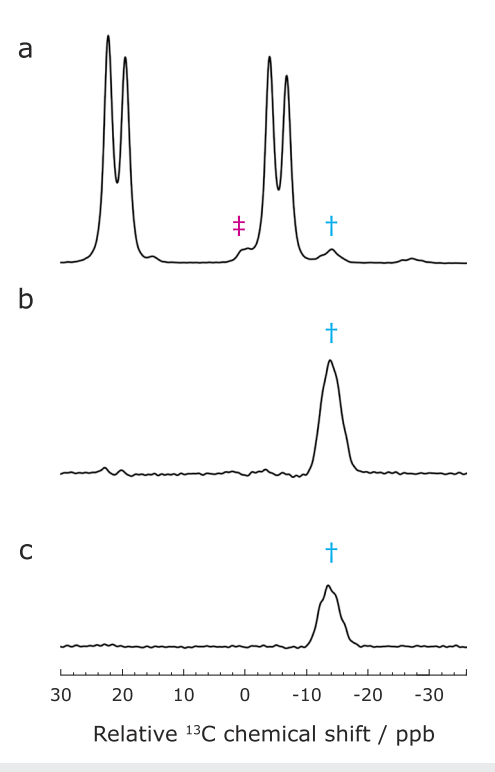


FIG. 9. Selective ¹³C NMR of 1,2 $^{-13}$ C $_2$ -squarate. All spectra are for a solution of 13 C $_1$ squarate at pH 13.3 and 298 K. The chemical shift scale is centered at 203.05 ppm. Blue dagger: 1,2 $^{-13}$ C $_2$ squarate signals; magenta double-dagger: 1,3 $^{-13}$ C $_2$ squarate signals. (a) A 90° pulse-acquire 13 C NMR spectrum of the 13 C $_2$ -squarate solution in a magnetic field of 9.4 T, averaged over 512 transients. (b) Double-quantum filtered spectrum obtained using the GeoDQ pulse sequence (1024 transients at 16.4 T), using parameters optimized for 1,2 $^{-13}$ C $_2$ -squarate (see Table III). (c) Singlet-filtered spectrum obtained using the GeoDQ-singlet pulse sequence (1024 transients at 16.4 T). The vertical scales of [(b) and (c)] are identical. The signal intensities of panel (a) cannot be compared directly with those of panels (b) and (c).

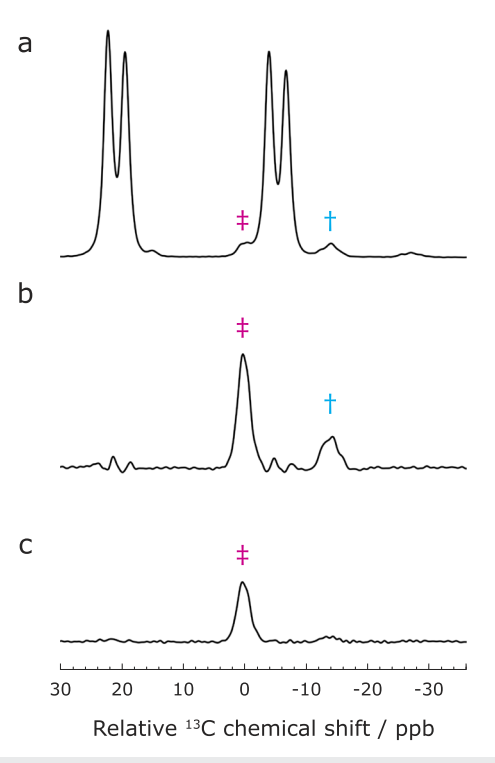


FIG. 10. Selective 13 C NMR of 1,3 $^{-13}$ C $_2$ -squarate. All spectra are for a solution of 13 C $_1$ squarate at pH 13.3 and 298 K. The chemical shift scale is centered at 203.05 ppm. Blue dagger: 1,2 $^{-13}$ C $_2$ squarate signals; magenta double-dagger: 1,3 $^{-13}$ C $_2$ squarate signals; magenta double-dagger: 1,3 $^{-13}$ C $_2$ squarate solution in a magnetic field of 9.4 T, averaged over 512 transients. (b) Double-quantum filtered spectrum obtained using the GeoDQ pulse sequence (1024 transients at 16.4 T), using parameters optimized for 1,3 $^{-13}$ C $_2$ -squarate (see Table III). (c) Singlet-filtered spectrum obtained using the GeoDQ-singlet pulse sequence (1024 transients at 16.4 T). The vertical scales of panels (b) and (c) are identical. The signal intensities of panel (a) cannot be compared directly to those of panels (b) and (c).

C. Double-quantum filtered singlet NMR

Geometric double-quantum filtration may be combined with singlet NMR in order to assess the singlet relaxation of the $1,2^{-13}C_2$ squarate and $1,3^{-13}C_2$ -squarate isotopologs, without interference from the much larger signals of the $^{13}C_2$ species.

The complete pulse sequence for double-quantum-filtered singlet NMR is shown in Fig. 11. The pulse sequence consists of eight consecutive elements.

- (i) Singlet-order-destruction (SOD). Longitudinal magnetization and singlet order are destroyed using a sequence of radio frequency pulses, delays, and field gradient pulses.²¹ The SOD sequence used in the current experiments is specified in the supplementary material.
- (ii) Geometric double-quantum excitation. After a delay for the establishment of longitudinal magnetization, a geometric double-quantum excitation sequence generates $^{13}C_2$ double-quantum coherence. The sequence used is given in Fig. 8, with the parameters for $1,2^{-13}C_2$ and $1,3^{-13}C_2$ squarate specified in Table III.

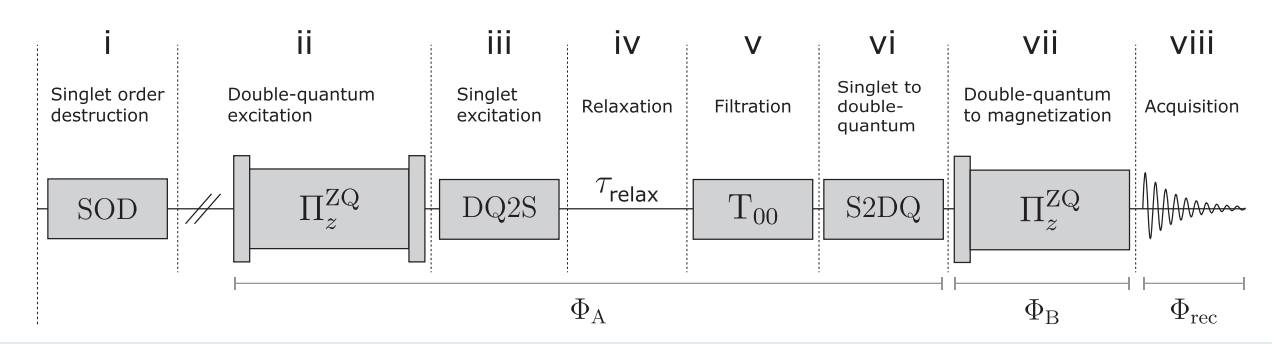


FIG. 11. Geometric double-quantum-filtering singlet pulse sequence. The pulse sequence elements are as follows: (i) the singlet-order destruction (SOD) block 21 removes any longitudinal magnetization and residual singlet order; (ii) following a relaxation delay to establish longitudinal magnetization, double-quantum coherence is generated by a geometric double-quantum excitation block, with an overall phase shift Φ_A ; (iii) a double-quantum-to-singlet (DQ2S) block converts double-quantum coherence to singlet order; (iv) singlet order decays during the relaxation interval τ_S ; (v) a T_{00} filter removes signals that do not pass through any rank-0 spherical tensor operators; (vi) a singlet-to-double-quantum (S2DQ) block converts singlet order to double-quantum coherence; (vii) a second geometric double-quantum pulse block is applied, with an overall phase Φ_B ; and (viii) the NMR signal is acquired and digitized, with receiver phase Φ_{rec} . The phases of the blocks are cycled as an overall four-step cycle: $\Phi_A = \{0,0,0,0\}, \Phi_B = \{0,\pi/2,\pi,3\pi/2\}, \text{ and } \Phi_{rec} = \{0,3\pi/2,\pi,\pi/2\}.$

- (iii) Double-quantum-to-singlet conversion (DQ2S). This pulse sequence block is shown in Fig. 12(a). This consists of an initial $\pi/2$ pulse with phase $-\pi/2$, followed by a $\pi/4$ pulse with phase 0, followed by a *J*-synchronized spin echo sequence, of similar type to that used in the M2S pulse sequence for converting longitudinal magnetization into singlet order. The operation of this sequence is described in the following.
- (iv) The singlet order is allowed to decay for a variable interval $\tau_{\rm relax}.$
- (v) A T₀₀ filter block suppresses all signals that do not pass through rank-0 spherical tensor order. ^{15,24} Since singlet order is described by a rank-0 spherical tensor operator, signals deriving from ¹³C₂ singlet order pass through the filter, while spurious signals from magnetization components are suppressed. The sequence used in the current experiments is specified in the supplementary material.
- (vi) A singlet-to-double-quantum (S2DQ) sequence converts singlet order back into double-quantum coherence. This pulse

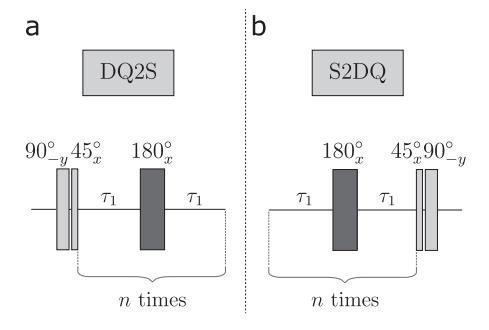


FIG. 12. (a) Double-quantum to singlet (DQ2S) block converts double-quantum coherence into singlet order. (b) The singlet to double-quantum (S2DQ) block is the chronological reverse of the DQ2S block and converts singlet order back to double-quantum coherence. The darker color indicates the implementation of a composite 180° pulse.⁵³ The parameters used in the experiments are given in Table III

- sequence block is shown in Fig. 12(b) and is the chronological reverse of the DQ2S sequence.
- (vii) A second geometric double-quantum sequence converts the double-quantum coherence into observable transverse magnetization. The sequences used are as in Fig. 8. The pulse sequence parameters for 1,2-13C2 and 1,3-13C2-squarate are specified in Table III.
- (viii) The 13 C NMR signal is observed with a receiver phase Φ_{rec} .

The phases Φ_A and Φ_B of the pulse sequence blocks and the receiver phase Φ_{rec} are cycled in subsequent transients, in order to suppress signals that do not pass through $^{13}C_2$ double-quantum coherences. The relaxation interval τ_{relax} is varied in a series of experiments in order to study the decay of $^{13}C_2$ singlet order in the two isotopomers.

The DQ2S pulse sequence block is shown in Fig. 12(a). The theoretical values of τ_1 and n are as given in Eq. (8). The experimentally optimized values are given in Table III.

The sequence operates as follows: the double-quantum spin density operator, generated by the GeoDQ sequence, has the following form (omitting the unity operator and numerical factors):⁴⁷

$$\rho_0 = i|T_{-1}\rangle\langle T_{+1}| - i|T_{+1}\rangle\langle T_{-1}|. \tag{9}$$

This has the following matrix representation, in the basis of singlet and triplet states [Eq. (1)]:

$$\rho_0 = i \begin{pmatrix} 0 & 0 & 0 & 0 \\ 0 & 0 & 0 & -1 \\ 0 & 0 & 0 & 0 \\ 0 & +1 & 0 & 0 \end{pmatrix}. \tag{10}$$

The first $\pi/2$ pulse of the DQ2S block converts the double-quantum coherence into antiphase triplet–triplet coherence,

$$\rho_1 = R_y(-\pi/2)\rho_0 R_y(+\pi/2) = \frac{i}{\sqrt{2}} \begin{pmatrix} 0 & 0 & 0 & 0\\ 0 & 0 & -1 & 0\\ 0 & +1 & 0 & +1\\ 0 & 0 & -1 & 0 \end{pmatrix}. \tag{11}$$

The $\pi/4$ pulse converts this into a state in which the central triplet state has a depleted population, relative to the two outer triplet states,

$$\rho_2 = R_x(\pi/4)\rho_1 R_x(-\pi/4) = \frac{1}{2} \begin{pmatrix} 0 & 0 & 0 & 0 \\ 0 & +1 & 0 & +1 \\ 0 & 0 & -2 & 0 \\ 0 & +1 & 0 & +1 \end{pmatrix}. \tag{12}$$

The next element of the DQ2S sequence is a J-synchronized multiple spin echo sequence, as shown in Fig. 12(a). The intervals τ_1 are given in Eq. (8).

As described in several places, 8,11 a J-synchronized spin echo sequence of suitable duration induces a rotation through π about the x axis of the zero-quantum subspace spanned by the $|S_0\rangle$, $|T_0\rangle$ states. This transformation exchanges the populations of the singlet and central triplet states, leading to the following density operator:

$$\rho_{3} = R_{x}^{\mathrm{ZQ}}(\pi)\rho_{2}R_{x}^{\mathrm{ZQ}}(-\pi) = \frac{1}{2} \begin{pmatrix} -2 & 0 & 0 & 0 \\ 0 & +1 & 0 & +1 \\ 0 & 0 & 0 & 0 \\ 0 & +1 & 0 & +1 \end{pmatrix}. \tag{13}$$

The state ρ_3 contains a component of singlet order since the mean population of the three triplet states (= 1/3) differs from the population of the singlet state (= -1). Hence, the sequence of manipulations in Fig. 12(a) converts double-quantum coherence into singlet order. The reverse sequence S2DQ [Fig. 12(b)] accomplishes the opposite transformation.

The overall theoretical efficiency for the DQ2S/S2DQ sequences to convert double-quantum coherence into singlet order, and back to double-quantum coherence again, is 2/3. This is the maximum achievable by consecutive unitary transformations. ^{60,61}

Figures 9(c) and 10(c) show 13 C NMR spectra acquired by using the pulse sequence in Fig. 11, but with no relaxation delays $\tau_{\rm relax}$. These NMR signals derive from the 13 C magnetization of the 13 C₂-squarate isotopologs, which have passed through both double-quantum coherence and singlet order. The sequences are seen to be highly selective and efficient. The nuclear spin order of the 13 C₂ pairs passes through double-quantum coherence to singlet order, and back again, with the retained amplitude not greatly less than the theoretical bound of 2/3.

D. Relaxation measurements

The relaxation interval $\tau_{\rm relax}$ of the pulse sequence shown in Fig. 11 was varied in a series of experiments in order to study the decay of $^{13}{\rm C}_2$ singlet order in the two isotopomers. The results obtained on a degassed solution at a magnetic field of 16.4T are shown in Fig. 13. The $^{13}{\rm C}_2$ singlet decay of the 1,2 $^{-13}{\rm C}_2$ -squarate isotopolog ($T_S \simeq 125 \pm 20{\rm s}$) is faster than that of the 1,3 $^{-13}{\rm C}_2$ -squarate isotopolog ($T_S \simeq 125 \pm 20{\rm s}$). This observation is in line with the molecular inversion symmetry of the 1,3 $^{-13}{\rm C}_2$ -squarate isotopolog, which cancels out the chemical shift anisotropy mechanism.

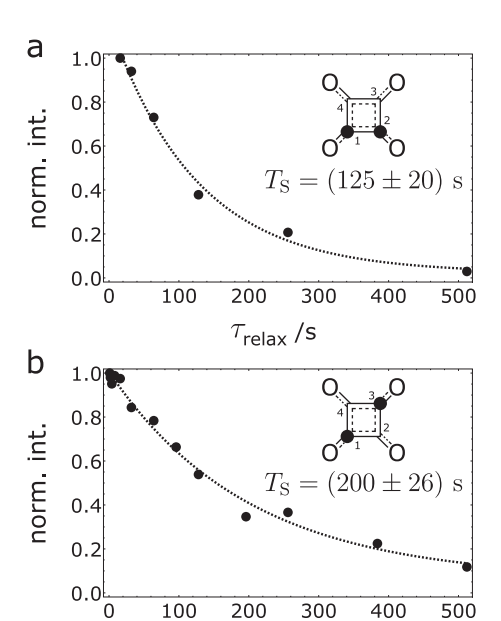


FIG. 13. (a) Decay curve for the $^{13}C_2$ singlet order of the $1,2-^{13}C_2$ -squarate isotopolog. (b) Decay curve for the $^{13}C_2$ singlet order of the $1,3-^{13}C_2$ -squarate isotopolog. All results were obtained on a degassed solution of $^{13}C_2$ -squarate in a field of 16.4 T at a temperature of 298 K, using the double-quantum-filtered singlet pulse sequence in Fig. 11. The dotted lines are best fits to single-exponential decays of the signal intensities.

 $au_{
m relax}$ /s

The singlet decay may be compared to the T_1 values for the decay of longitudinal magnetization for the same isotopologs, which were estimated by using a standard inversion-recovery sequence, followed by geometric double-quantum filtration in order to selectively observe the relaxation of the $1,2^{-13}C_2$ or $1,3^{-13}C_2$ -squarate signals. The observed T_1 values were $29 \pm 1s$ in both cases, indicating that the singlet order decay is between 6 and 10 times slower than that of the longitudinal magnetization for the species.

IV. DISCUSSION

The squarate dianion presents an unusual example of high local symmetry and the absence of magnetic nuclei in the most abundant natural isotopolog. By synthetically introducing a single $^{13}\mathrm{C}$ label into each molecule, and using double-quantum techniques, it is possible to study low-abundance $^{13}\mathrm{C}_2$ isotopologs in which the $^{13}\mathrm{C}$ nuclei are either at adjacent molecular positions (in the case of $1,2^{-13}\mathrm{C}_2$ -squarate) or at inversion-related molecular positions (in the case of $1,3^{-13}\mathrm{C}_2$ -squarate). Long-lived $^{13}\mathrm{C}_2$ singlet order may be accessed in these isotopologs by introducing $^{18}\mathrm{O}$ nuclei, which have no magnetic moment but slightly modify the $^{13}\mathrm{C}$ chemical shifts through the mass difference between $^{16}\mathrm{O}$ and $^{18}\mathrm{O}$.

The ¹³C NMR spectrum of ¹⁸O-enriched ¹³C-squarate presents a rich multiplet structure due to the large number of isotopologs and the plethora of secondary isotope shifts. The ¹⁸O-induced ¹³C isotope shifts are observed to be strongly pH-dependent. These pH-dependent isotope shifts are attributed to a superposition of the

vibronic and dynamic isotope shift mechanisms. In the dynamic mechanism, the substitution of an ¹⁶O atom by an ¹⁸O atom at a molecular protonation site perturbs the average ¹³C chemical shifts throughout the molecule by slightly shifting the acid-base equilibrium.

At high pH, the dynamic contribution to the isotope shifts vanishes since the squarate dianion $C_4O_4^{2^-}$ is the only significant species in solution. The remaining vibronic shifts display an unexpected property: the two-bond $^2\Delta^{13}C(^{18}O)$ secondary isotope shift is negligibly small, unlike both the one-bond shift $^1\Delta^{13}C(^{18}O)$ and the three-bond shift $^3\Delta^{13}C(^{18}O)$. The very small value of the two-bond isotope shift is unexplained at the current time.

The 18 O-induced 13 C isotope shifts allow the use of geometric double-quantum-filtering to selectively detect the signals from the minor 1 ,2 $^{-13}$ C₂ and 1 ,3 $^{-13}$ C₂-squarate isotopologs, with good suppression of the much larger signals from the 13 C₂ species. The conversion of 13 C₂ double-quantum coherence into 13 C₂ singlet order, and back again, was demonstrated with good efficiency by using novel DQ2S and S2DQ procedures.

As expected, the singlet relaxation time constants T_S were found to greatly exceed the T_1 values, for both the $1,2^{-13}C_2$ -squarate and the $1,3^{-13}C_2$ -squarate isotopologs. The T_S time constant for $1,3^{-13}C_2$ -squarate was measured to be ~200 s in high-pH aqueous solution, in the high magnetic field of 16.4T. The long singlet relaxation time may be attributed to the inversion symmetry of this molecular species, which causes excellent suppression of the large chemical shift anisotropy mechanism, even in high magnetic field. Nevertheless, although the T_S time constant is unusually long for a species in high magnetic field in aqueous solution, it seems that intermolecular interactions with solvent protons and other species, combined with the relatively high viscosity of the aqueous environment, still limit the singlet relaxation time to a few minutes, even for this highly favorable species.

SUPPLEMENTARY MATERIAL

The supplementary material provides (1) computational chemistry calculations of the CSA tensors and the *J*-couplings; (2) additional pulse sequence details.

ACKNOWLEDGEMENTS

We acknowledge funding received from the European Research Council (Grant No. 786707-FunMagResBeacons) and EPSRC-UK (Grant Nos. EP/P030491/1 and EP/V055593/1).

AUTHOR DECLARATIONS

Conflict of Interest

The authors have no conflicts to disclose.

Author Contributions

Urvashi D. Heramun: Data curation (equal); Formal analysis (equal); Investigation (lead); Validation (equal); Visualization (lead);

Writing – original draft (equal); Writing – review & editing (equal). Mohamed Sabba: Conceptualization (equal); Formal analysis (supporting); Methodology (equal); Supervision (supporting); Validation (equal); Writing – review & editing (supporting). Christian Bengs: Conceptualization (equal); Formal analysis (supporting); Methodology (equal); Software (equal); Supervision (supporting); Validation (equal); Writing – review & editing (supporting). Gamal A. I. Moustafa: Resources (lead). Malcolm H. Levitt: Conceptualization (equal); Data curation (equal); Formal analysis (equal); Funding acquisition (lead); Project administration (lead); Software (equal); Supervision (lead); Validation (equal); Writing – original draft (equal); Writing – review & editing (equal).

DATA AVAILABILITY

The data that support the findings of this study are available from the corresponding author upon reasonable request. The pulse sequences used were deposited and made available with the assigned DOI: https://doi.org/10.5258/SOTON/D3557.

REFERENCES

- ¹M. Carravetta, O. G. Johannessen, and M. H. Levitt, Phys. Rev. Lett. **92**, 153003 (2004).
- ²M. Carravetta and M. H. Levitt, J. Am. Chem. Soc. 126, 6228 (2004).
- ³S. Cavadini, J. Dittmer, S. Antonijevic, and G. Bodenhausen, J. Am. Chem. Soc. 127, 15744 (2005).
- ⁴G. Pileio, M. Concistrè, M. Carravetta, and M. H. Levitt, J. Magn. Reson. **182**, 353 (2006).
- ⁵E. Vinogradov and A. K. Grant, J. Magn. Reson. 188, 176 (2007).
- ⁶P. Ahuja, R. Sarkar, P. R. Vasos, and G. Bodenhausen, J. Chem. Phys. 127, 134112 (2007).
- ⁷W. S. Warren, E. Jenista, R. T. Branca, and X. Chen, Science 323, 1711 (2009).
- ⁸G. Pileio, M. Carravetta, and M. H. Levitt, Proc. Natl. Acad. Sci. U. S. A. 107, 17135 (2010).
- ⁹G. Pileio and M. H. Levitt, J. Chem. Phys. **130**, 214501 (2009).
- ¹⁰G. Pileio, Prog. Nucl. Magn. Reson. Spectrosc. **56**, 217 (2010).
- ¹¹ M. C. D. Tayler and M. H. Levitt, Phys. Chem. Chem. Phys. 13, 5556 (2011).
- ¹²G. Pileio, J. T. Hill-Cousins, S. Mitchell, I. Kuprov, L. J. Brown, R. C. D. Brown, and M. H. Levitt, J. Am. Chem. Soc. 134, 17494 (2012).
- ¹³ M. H. Levitt, Annu. Rev. Phys. Chem. **63**, 89 (2012).
- ¹⁴S. J. DeVience, R. L. Walsworth, and M. S. Rosen, Phys. Rev. Lett. **111**, 173002 (2013).
- ¹⁵M. C. D. Tayler and M. H. Levitt, J. Am. Chem. Soc. **135**, 2120 (2013).
- ¹⁶ J.-N. Dumez, P. Håkansson, S. Mamone, B. Meier, G. Stevanato, J. T. Hill-Cousins, S. S. Roy, R. C. D. Brown, G. Pileio, and M. H. Levitt, J. Chem. Phys. 142, 044506 (2015).
- ¹⁷G. Stevanato, S. Singha Roy, J. Hill-Cousins, I. Kuprov, L. J. Brown, R. C. D. Brown, G. Pileio, and M. H. Levitt, Phys. Chem. Chem. Phys. 17, 5913 (2015).
- ¹⁸G. Stevanato, J. T. Hill-Cousins, P. Håkansson, S. S. Roy, L. J. Brown, R. C. D. Brown, G. Pileio, and M. H. Levitt, Angew. Chem. Int., Ed. 54, 3740 (2015).
- ¹⁹S. J. Elliott, L. J. Brown, J.-N. Dumez, and M. H. Levitt, J. Magn. Reson. **272**, 87 (2016).
- ²⁰M. H. Levitt, J. Magn. Reson. **306**, 69 (2019).
- ²¹B. A. Rodin, K. F. Sheberstov, A. S. Kiryutin, L. J. Brown, R. C. D. Brown, M. Sabba, M. H. Levitt, A. V. Yurkovskaya, and K. L. Ivanov, J. Chem. Phys. 151, 234203 (2019).
- ²² J.-N. Dumez, Mol. Phys. 118, e1644382 (2020).
- ²³S. Mamone, N. Rezaei-Ghaleh, F. Opazo, C. Griesinger, and S. Glöggler, Sci. Adv. 6, eaaz1955 (2020).

- ²⁴M. C. D. Tayler, in *Long-Lived Nuclear Spin Order: Theory and Applications*, edited by G. Pileio (Royal Society of Chemistry, 2020), pp. 188–208.
- ²⁵C. Bengs, L. Dagys, G. A. I. Moustafa, J. W. Whipham, M. Sabba, A. S. Kiryutin, K. L. Ivanov, and M. H. Levitt, J. Chem. Phys. 155, 124311 (2021).
- ²⁶ J. Eills, E. Cavallari, R. Kircher, G. Di Matteo, C. Carrera, L. Dagys, M. H. Levitt, K. L. Ivanov, S. Aime, F. Reineri, K. Münnemann, D. Budker, G. Buntkowsky, and S. Knecht, Angew. Chem., Int. Ed. 60, 6791 (2021).
- ²⁷S. Mamone, A. B. Schmidt, N. Schwaderlapp, T. Lange, D. von Elverfeldt, J. Hennig, and S. Glöggler, NMR Biomed. 34, e4400 (2021).
- ²⁸ A. Sonnefeld, A. Razanahoera, P. Pelupessy, G. Bodenhausen, and K. Sheberstov, Sci. Adv. 8, eade2113 (2022).
- ²⁹ X. Yang, K.-R. Hu, J.-X. Xin, Y.-X. Li, G. Yang, D.-X. Wei, and Y.-F. Yao, J. Magn. Reson. 338, 107188 (2022).
- ³⁰ A. Razanahoera, A. Sonnefeld, G. Bodenhausen, and K. Sheberstov, Magn. Reson. 4, 47 (2023).
- ³¹ D. H. Lysak, F. V. C. Kock, S. Mamone, R. Soong, S. Glöggler, and A. J. Simpson, Chem. Sci. **14**, 1413 (2023).
- ³²H. Harbor-Collins, M. Sabba, C. Bengs, G. Moustafa, M. Leutzsch, and M. H. Levitt, J. Chem. Phys. 160, 014305 (2024).
- ⁵³J. W. Whipham, M. Sabba, L. Dagys, G. Moustafa, C. Bengs, and M. H. Levitt, J. Chem. Phys. **161**, 014112 (2024).
- ³⁴P. R. Bunker and P. Jensen, *Fundamentals of Molecular Symmetry* (Institute of Physics, Bristol, 2005).
- 35 R. Radeglia, Solid State Nucl. Magn. Reson. 4(5), 317–321 (1995).
- ³⁶R. P. Young, C. R. Lewis, C. Yang, L. Wang, J. K. Harper, and L. J. Mueller, Magn. Reson. Chem. **57**, 211 (2019).
- ³⁷ A. D. Buckingham and S. M. Malm, Mol. Phys. **22**, 1127 (1971).
- ³⁸N. F. Ramsey, Phys. Rev. **87**, 1075 (1952).
- ³⁹H. Batiz-Hernandez and R. A. Bernheim, Prog. Nucl. Magn. Reson. Spectrosc. 3, 63 (1967).

- ⁴⁰C. J. Jameson, J. Chem. Phys. **66**, 4983 (1977).
- ⁴¹P. E. Hansen, Prog. Nucl. Magn. Reson. Spectrosc. 20, 207 (1988).
- ⁴²C. J. Jameson, *Isotopes in the Physical and Biomedical Science* (Elsevier Science, Amsterdam, Netherlands, 1991), Vol. 2.
- ⁴³P. Lantto, S. Kangasvieri, and J. Vaara, J. Chem. Phys. **137**, 214309 (2012).
- ⁴⁴P. Lantto, S. Kangasvieri, and J. Vaara, Phys. Chem. Chem. Phys. 15, 17468 (2013).
- ⁴⁵A. Bax, R. Freeman, and S. P. Kempsell, J. Am. Chem. Soc. **102**, 4849 (1980).
- ⁴⁶T. Nakai and C. A. Mcdowell, Mol. Phys. **79**, 965 (1993).
- ⁴⁷C. Bengs, M. Sabba, and M. H. Levitt, J. Chem. Phys. **158**, 124204 (2023).
- ⁴⁸S. L. R. Ellison and M. J. T. Robinson, J. Chem. Soc. Chem. Commun. **1983**, 745.
- 49 C. L. Perrin and J. D. Thoburn, J. Am. Chem. Soc. 114, 8559 (1992).
- ⁵⁰ W. Arias and J. M. Risley, J. Org. Chem. **56**, 3741 (1991).
- ⁵¹ T. L. Mega and R. L. Van Etten, J. Am. Chem. Soc. **115**, 12056 (1993).
- ⁵²B. N. Craig, M. U. Janssen, B. M. Wickersham, D. M. Rabb, P. S. Chang, and D. J. O'Leary, J. Org. Chem. **61**, 9610 (1996).
- ⁵³ M. H. Levitt and R. Freeman, J. Magn. Reson. 1969 **33**, 473 (1979).
- ⁵⁴ A. Bax, R. Freeman, T. A. Frenkiel, and M. H. Levitt, J. Magn. Reson. 1969 43, 478 (1981).
- ⁵⁵S. J. DeVience, R. L. Walsworth, and M. S. Rosen, NMR Biomed. **26**, 1204 (2013).
- ⁵⁶Y. Aharonov and J. Anandan, Phys. Rev. Lett. **58**, 1593 (1987).
- ⁵⁷ M. Berry, Proc. R. Soc. London A **392**, 45 (1984).
- ⁵⁸J. W. Zwanziger, M. Koenig, and A. Pines, Annu. Rev. Phys. Chem. 41, 601 (1990).
- 59 M. C. D. Tayler, "Theory and practice of singlet nuclear magnetic resonance," Ph.D. thesis, University of Southampton, 2012.
- ⁶⁰O. W. Sørensen, J. Magn. Reson. 1969 **86**, 435 (1990).
- ⁶¹ M. H. Levitt, J. Magn. Reson. 262, 91 (2016).